Multi-user cognitive radio network resource allocation based on the adaptive niche immune genetic algorithm*

Zu Yun-Xiao(祖云霄)† and Zhou Jie(周 杰)

School of Electronic Engineering, Beijing University of Posts and Telecommunications, Beijing 100876, *China*

(Received 13 December 2010; revised manuscript received 27 July 2011)

Multi-user cognitive radio network resource allocation based on the adaptive niche immune genetic algorithm is proposed, and a fitness function is provided. Simulations are conducted using the adaptive niche immune genetic algorithm, the simulated annealing algorithm, the quantum genetic algorithm and the simple genetic algorithm, respectively. The results show that the adaptive niche immune genetic algorithm performs better than the other three algorithms in terms of the multi-user cognitive radio network resource allocation, and has quick convergence speed and strong global searching capability, which effectively reduces the system power consumption and bit error rate.

Keywords: cognitive radio networks, niche genetic algorithm, King map, resource allocation

PACS: 95.85.Bh **DOI:** 10.1088/1674-1056/21/1/019501

1. Introduction

The cognitive radio network was originally suggested by Joseph[1] in 1999, and has the ability to sense and learn the current status of the surrounding wireless environment in order to make full use of the idle spectrum. The resource allocation of the cognitive radio network is a key technology. It achieves dynamic spectrum allocation and system resource schedule by intellective learning and the heuristic algorithm.[2−5] As the system parameters, such as transmission power, carrier frequency and modulation order, dynamically change, the cognitive radio network can effectively adapt to the changes in the wireless environment and achieve a high reliable communication, as well as an effective use of the limited radio spectrum resources in space.

The previous research developed a simple genetic algorithm (SGA) for multi-user cognitive radio network resource allocation,[6] which focuses on multi-carrier power control and adaptive subcarrier-bit allocation. The algorithm gives an almost optimal performance after carrying out a large number of iterations, but it has a slow convergence speed, so it is hard to use in practical systems. The resource allocation and schedule, in which the simulated annealing algorithm (SA) is used, is presented in Ref. [7]. The bit error rate (BER) reduction is expected by using the algorithm for dynamic modulation and subcarrier allocation, but the computational complexity is very high. The quantum genetic algorithm (QGA) in Ref. [8] dynamically allocated the radio spectrum to each user, and had a high convergence speed, but it did not analyse the ratio of per-bit energy to noise power spectral density $E_{\rm b}/N_0$.

In this paper, a novel resource allocation method based on the adaptive niche immune genetic algorithm (ANIGA) is proposed for multi-user cognitive radio networks. We establish a simulation platform and compare ANIGA with SGA, QGA and SA in multi-user cognitive radio networks. The simulation results show that ANIGA performs better than the other three algorithms. It has a quick convergence speed and a strong global searching capability, which also reduces the system power consumption and the BER effectively.

The rest of this paper is organized as follows. In Section 2 a system model of the multi-user cognitive radio network resource allocation is presented, and a fitness function is provided. In Section 3 a resource allocation method based on ANIGA is presented, and the simulation results and analysis are presented in Section 4. The conclusion is given in Section 5.

*Project supported by the Research Fund for Joint China–Canada Research and Development Projects of the Ministry of Science and Technology, China (Grant No. 2010DFA11320).

†Corresponding author. E-mail: zuyx@tsinghua.edu.cn

© 2012 Chinese Physical Society and IOP Publishing Ltd

2. The resource allocation model for multi-user cognitive radio networks

The spectrum resource model of the cognitive radio network is shown in Fig. 1. With smart spectrum sense technology, the secondary users can use the idle spectrum, which is not in deep fading for all secondary users or occupied by the primary users. We focus on the cognitive radio network using orthogonal frequency-division multiple access technology, which accumulates all available idle spectra into a spectrum pool and divides the spectrum pool into orthogonal sub-carriers. The system combines several adjacent sub-carriers into one logic sub-channel, and then allocates it to a single secondary user. Since the adjacent sub-carriers all have similar frequencies, correspondingly, they will have similar channel gains to the same user, which can be considered to be flat fading. According to the channel gain and the rate demand of different secondary users, the cognitive radio network dynamically adjusts the modulation order of the sub-channels. After that, the system will dynamically allocate the available sub-channels to different secondary users.

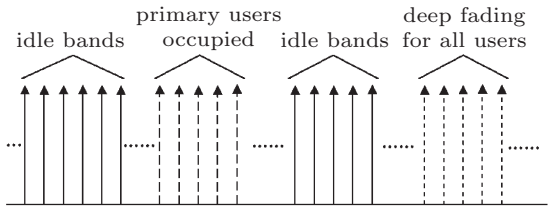


Fig. 1. The spectrum resource model.

In this article, we aim to maximize the total transmission rate for the secondary users in the cognitive radio networks with the constraints of the limited transmission power, the demand for secondary user rate and the BER. We assume that there are N available idle sub-carriers and K secondary users, and the total transmission rate of the cognitive radio network can be shown as

$$\max R = L\sum_{n=1}^{N}\sum_{k=1}^{K} m_{k,n}, \tag{1}$$

where R denotes the total transmission rate in the cognitive radio network, L is the bandwidth of each sub-carrier and $m_{k,n}$ is the modulation order of the k-th secondary user on the n-th sub-carrier. With the constraint of system maximum transmission power $P_{\max}$, the total transmission power of the secondary users must satisfy the constraint

$$\sum_{n=1}^{N}\sum_{k=1}^{K} L\frac{f(m_{k,n},P_{\rm e})}{a_{k,n}^2} \le P_{\max}, \tag{2}$$

where $a_{k,n}$ denotes the channel gain of the k-th user on the n-th sub-carrier, and $f(m_{k,n},P_{\rm e})$ represents the power consumption by the k-th secondary user on sub-carrier n with modulation order $m_{k,n}$ under the BER constraint $P_{\rm e}$. It is given by

$$f(m_{k,n},P_{\rm e}) = \frac{N_0}{3}\left[Q^{-1}\left(\frac{P_{\rm e}}{4}\right)\right]^2(2^{m_{k,n}}-1), \tag{3}$$

where $Q(x)$ is the normal distribution integral function, which can be expressed as

$$Q(x) = \frac{1}{\sqrt{2\pi}}\int_x^{\infty} {\rm e}^{-t^2/2}{\rm d}t. \tag{4}$$

Because each sub-channel must be assigned to only one secondary user to avoid spectrum conflict, we assume that the user number is k_0, so the second constraint is given by

$$m_{k,n} = \begin{cases} m_{k_0,n}, & (k=k_0), \\ 0, & (k\ne k_0), \end{cases} \quad n\in\{1,2,\cdots,N\}. \tag{5}$$

Each secondary user must meet the minimum rate demand, so the third constraint can be shown to be

$$L\sum_{n=1}^{N} m_{k,n} \ge R_k, \quad k\in\{1,2,\cdots,K\}, \tag{6}$$

where R_k denotes the minimum rate demand from the k-th secondary user.

3. Resource allocation for multi-user cognitive radio networks based on ANIGA

3.1. ANIGA

In this paper, we propose ANIGA for multi-user cognitive radio network resource allocation. The traditional immune genetic algorithm (IGA) is an improved genetic algorithm based on the creature immune mechanism, which maps the objective function and the solution of a problem to an antigen and the corresponding antibody, respectively. However, traditional IGA has its disadvantages, such as a simple memory cell, a single antibody population space and fixed parameters, which can easily lead to premature and slow convergence. By adaptively updating

the memory cells, establishing niche sub-populations and dynamically adjusting the crossover and mutation parameters, ANIGA can effectively improve the global search ability, accelerate the convergence speed and avoid premature convergence. The key steps of ANIGA include encoding the antigen and the antibody, generating the initial antibody population, dynamically adjusting the sub-population size, crossing over, mutating, adaptively adjusting the parameters and updating the memory cells.

3.2. The encoding antigen and antibody

In ANIGA, the fitness function and the antigen for the multi-user cognitive radio network resource allocation can be given as

$$\begin{aligned} &\max R = L\sum_{n=1}^{N}\sum_{k=1}^{K} m_{k,n} \\ &\text{s.t} \quad \sum_{n=1}^{N}\sum_{k=1}^{K} L\frac{f(m_{k,n},P_{\mathrm{e}})}{a_{k,n}^2} \le P_{\max}, \\ &L\sum_{n=1}^{N} m_{k,n} \ge R_k, \quad k\in\{1,2,\cdots,K\}. \end{aligned} \tag{7}$$

In order to facilitate the crossover and mutation operations, we use the matrix form to represent the channel gain. Assuming that there are K secondary users and N sub-carriers in the cognitive radio network, the channel gain matrix can be given as

$$\boldsymbol{G} = \begin{bmatrix} g_{1,1} & g_{1,2} & \cdots & g_{1,N-1} & g_{1,N} \\ g_{2,1} & g_{2,2} & \cdots & g_{2,N-1} & g_{2,N} \\ \vdots & \vdots & \ddots & \vdots & \vdots \\ g_{K-1,1} & g_{K-1,2} & \cdots & g_{K-1,N-1} & g_{K-1,N} \\ g_{K,1} & g_{K,1} & \cdots & g_{K,N-1} & g_{K,N} \end{bmatrix}, \tag{8}$$

where $g_{k,n} = 1/a_{k,n}^2$ represents the channel fading of the k-th user on the n-th sub-carrier. The antibody matrix $\boldsymbol{M}$ is given as

$$\boldsymbol{M} = \begin{bmatrix} m_{1,1} & m_{1,2} & \cdots & m_{1,N-1} & m_{1,N} \\ m_{2,1} & m_{2,2} & \cdots & m_{2,N-1} & m_{2,N} \\ \vdots & \vdots & \ddots & \vdots & \vdots \\ m_{K-1,1} & m_{K-1,2} & \cdots & m_{K-1,N-1} & m_{K-1,N} \\ m_{K,1} & m_{K,1} & \cdots & m_{K,N-1} & m_{K,N} \end{bmatrix}, \tag{9}$$

which represents the solution to the multi-user cognitive radio network resource allocation problem. Each sub-carrier can be occupied by only one secondary user, so there is only one non-zero value in each column of matrix $\boldsymbol{M}$. The aim of ANIGA is to find the antibody with the highest fitness value, which means the best modulation order and the optimum allocation of sub-carriers to the secondary users.

3.3. Generating the initial antibody population

In ANIGA, the three-dimensional King map is used to generate the initial antibody population.[9−17] The three-dimensional King map can be expressed as

$$\begin{cases} x_{n+1} = \sin(ay_n) - z_n\cos(bx_n), \\ y_{n+1} = z_n\sin(cx_n) + \cos(dy_n), \\ z_{n+1} = e\sin(x_n), \end{cases} \tag{10}$$

where a, b, c, d and e are constant coefficients. When $a = 2.24$, $b = 0.43$, $c = -0.65$, $d = -2.43$, $e = 0.7$ and initial point $(x_0, y_0, z_0) = (0.1, 0.1, 0.1)$, the system is in a complete chaotic state.[18−26] In order to initialize the antibody population, the elements of the antibody matrix can be assigned as

$$\begin{cases} m_{k,n} = \left\lfloor \frac{(H+1)\cdot x_n}{2} \right\rfloor, & (k = k_0), \\ m_{k,n} = 0, & (k \ne k_0), \end{cases} \tag{11}$$

where $\lfloor\ \rfloor$ represents taking a round integer downward, H is the highest modulation order of the system and k_0 is the user number, which can be given as

$$k_0 = \left\lfloor \frac{(K+1)y_n}{2} \right\rfloor. \tag{12}$$

We use the King map chaotic sequence to complete the initialization,[27−32] and the individuals in the initial population will maintain a high degree of uniformity and randomness,[33−48] which will speed up the convergence rate in the initial stage of ANIGA.

3.4. Dynamically adjusting the sub-population size

In the traditional IGA, only one antibody population is set up, which easily leads to a premature convergence.[49−56] In ANIGA, the antibody population is divided into multiple independent sub-populations, and each sub-population contains multiple antibodies. In this way, each sub-population can evolve independently and maintain the competition. This method not only avoids the occurrence of premature convergence, but also speeds up the process of antibody evolution.

Traditionally, the dynamic change in the sub-population size is proportional to the average fitness of

the antibodies. However, in this method, the similarity between the antibodies is not taken into consideration, which leads to a large number of highly similar antibodies that occupy the entire sub-population and continuously expand the scale of the sub-population. In this paper, we present a method that considers the antibody density and averages the fitness to dynamically change the size of the sub-population, which can be given as

$$n_k(t+1) = C \times \frac{(1-\rho_k(t))f_k^{\mathrm{a}}(t)}{\sum_{i=1}^{K}(1-\rho_i(t))f_i^{\mathrm{a}}(t)}, \tag{13}$$

where C is the total number of antibodies in the population, $n_k(t+1)$ is the scale of the k-th sub-population after $t+1$ iterations, and $f_k^{\mathrm{a}}(t)$ and $\rho_k(t)$ represent the average fitness and the antibody density of the k-th sub-population after t iterations, respectively. They are given by

$$f_k^{\mathrm{a}}(t) = \sum_{i=1}^{n_k(t)} f_{ki}(t)/n_k(t), \tag{14}$$

$$\rho_k(t) = \frac{s_k(t)_{\mathrm{similar}}}{n_k(t)}, \tag{15}$$

where $n_k(t)$ is the number of antibodies in the sub-population, $f_{ki}(t)$ is the fitness of the i-th antibody in the k-th sub-population and $s_k(t)_{\mathrm{similar}}$ is the number of antibodies with a high degree of similarity. The Hamming distance of two antibodies is given by

$$||z_i - z_j|| = \sqrt{\sum_{k=1}^{D}(z_{ik} - z_{jk})^2}, \quad (i \neq j), \tag{16}$$

where D is the length of the antibody genes, and z_{ik} and z_{jk} are the genes at position k belonging to antibodies z_i and z_j, respectively. When the Hamming distance between two antibodies is less than a certain value, we consider the two antibodies with a high degree of similarity.

3.5. Crossover and mutation

Since the number of sub-carriers in the multi-user cognitive radio network is very large, the antibody matrix has a large number of columns. For this reason, the traditional single-point crossover will lead to a slow convergence and result in evolutionary stagnation. In ANIGA, a three-point crossover operator is used to exchange adjacent gene sequences, with the location selected by the chaotic sequence, which can be shown in Fig. 2.

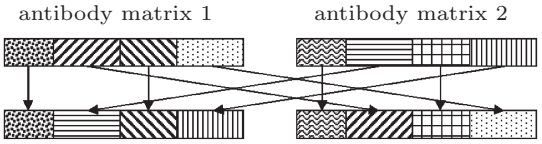


Fig. 2. The three-point crossover.

Figure 2 shows the process in which the three-point crossover operation is applied to two antibody matrices. As can be seen from Fig. 2, two antibodies exchange genes at the corresponding positions by crossover operation. The crossover operation produces two new antibody matrices, which represent two new resource allocation schemes.

In order to generate new genes and avoid evolutionary stagnation, in ANIGA a small proportion of antibodies are randomly selected to perform the mutation operation. The mutation operation swaps two random rows of the selected antibody matrix, as shown in Fig. 3.

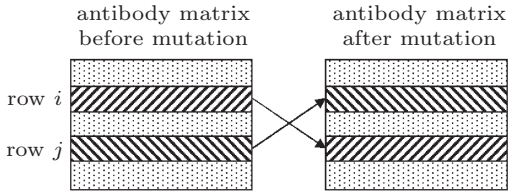


Fig. 3. The mutation operation.

In Fig. 3, the mutation operation makes the i-th row and the j-th row swap with each other, which generates new genes and produces a new antibody matrix. After the mutation operation, each column of the antibody matrix contains only one non-zero element, which ensures that each sub-carrier is allocated to only one secondary user.

3.6. Adaptively adjusting parameters

In order to enhance the convergence speed, we adaptively adjust the probability of the crossover operation, which is given by

$$P_{\mathrm{crossover}}(\boldsymbol{M}_i, \boldsymbol{M}_j) = k_1 \frac{2f_{\max} - f(\boldsymbol{M}_i) - f(\boldsymbol{M}_j)}{f_{\max} - f_{\min}}, \tag{17}$$

where k_1 is a constant coefficient, $f(\boldsymbol{M}_i)$ and $f(\boldsymbol{M}_j)$ are the fitness values of two antibodies $\boldsymbol{M}_i$ and $\boldsymbol{M}_j$, respectively, $f_{\max}$ is the largest fitness value and $f_{\min}$ is the smallest fitness value in the sub-population.

As shown in formula (17), the crossover probability P_{cross} is adaptively adjusted according to the values of $f(\boldsymbol{M}_i)$, $f(\boldsymbol{M}_j)$, $f_{\max}$, and $f_{\min}$.

Through adaptive adjustment of the crossover probability, the antibodies with high fitness are more likely to skip the crossover and be retained for the next generation, and the antibodies with low fitness are given higher crossover probabilities, which are more likely to be restructured and used to generate new genes.

The mutation probability is given by

$$P_{\text{mutation}}(\boldsymbol{M}_i) = k_2 \frac{f_{\max} - f(\boldsymbol{M}_i)}{f_{\max} - f_{\min}}, \tag{18}$$

which is adaptively adjusted with antibody fitness $f(\boldsymbol{M}_i)$, $f_{\max}$ and $f_{\min}$ in the sub-population. In this way, the low fitness antibodies will have higher mutation probabilities, which will generate new genes and improve the overall fitness of the antibody population.

3.7. Updating the memory cells

In the traditional IGA, the memory cell will be periodically updated, and the high fitness antibodies will be retained in the memory cell. However, there is only one single memory cell space, so the algorithm can easily to fall into a suboptimal solution rather than a global optimal one.

In ANIGA, several independent memory cells are set up, which prevents the algorithm from falling into the suboptimal solution. In the update process of the memory cells, the multi-island model is used, which adjusts the size of the memory cell proportional to the average fitness of the antibody. In adjacent memory cells, antibody information is exchanged periodically, which can speed up the convergence rate and obtain a global optimal solution.

4. Simulation and analysis

4.1. The basic steps of ANIGA

A basic flow chart of ANIGA is shown in Fig. 4. First we generate the initial antibodies with the memory cells and the chaotic sequence. After that the antibody population will be divided into multiple sub-populations. Then we will calculate antibody fitness within the sub-populations and update the memory cell with high fitness antibodies. The algorithm then dynamically changes the size of the sub-populations and adjusts the parameters of crossover and mutation according to the fitness value. Finally, we check whether the algorithm has arrived at the designated iterations. If so, the antibody with the highest fitness will be output, otherwise the process in the flow chart will be continued.

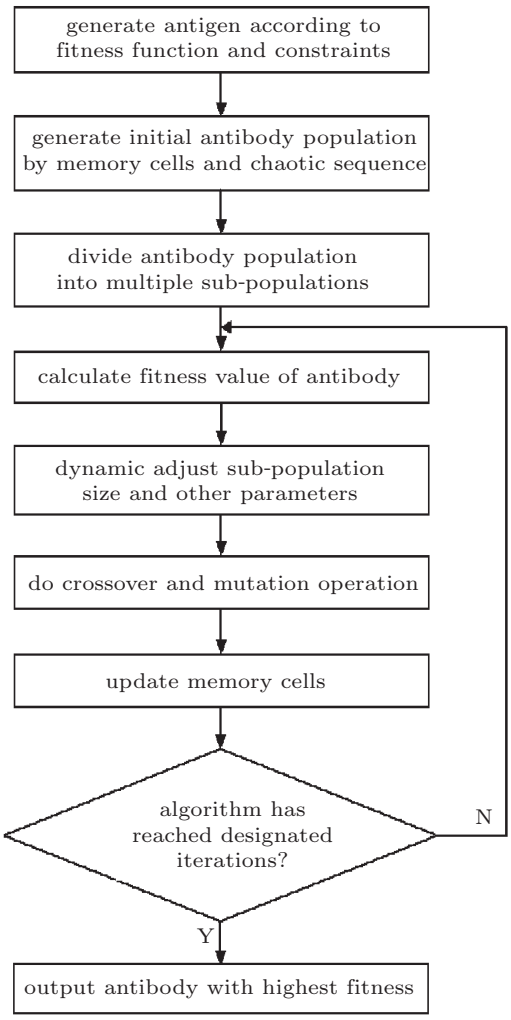


Fig. 4. The basic steps of ANIGA.

4.2. Simulation results and analysis

In the simulation, we assume that the channel estimation is accurate, the single-side power spectral density of the additive white Gaussian noise channel is $N_0 = 1$, the total idle spectrum bandwidth of the spectrum pool is 15 MHz, the number of sub-carriers is 1024, the bandwidth of each sub-carrier is 15 kHz and each user's rate demand is 6 Mbps. The modulation modes are BPSK, QPSK and 16, 32, 64, 128 and 256 QAM, which means that the maximum modulation order is 8 bit·s^{-1}·Hz^{-1}. In ANIGA, we set the population size to be 64, the generation gap 0.8, the maximum generation 1000, the crossover probability 0.7 and the mutation probability 0.05.

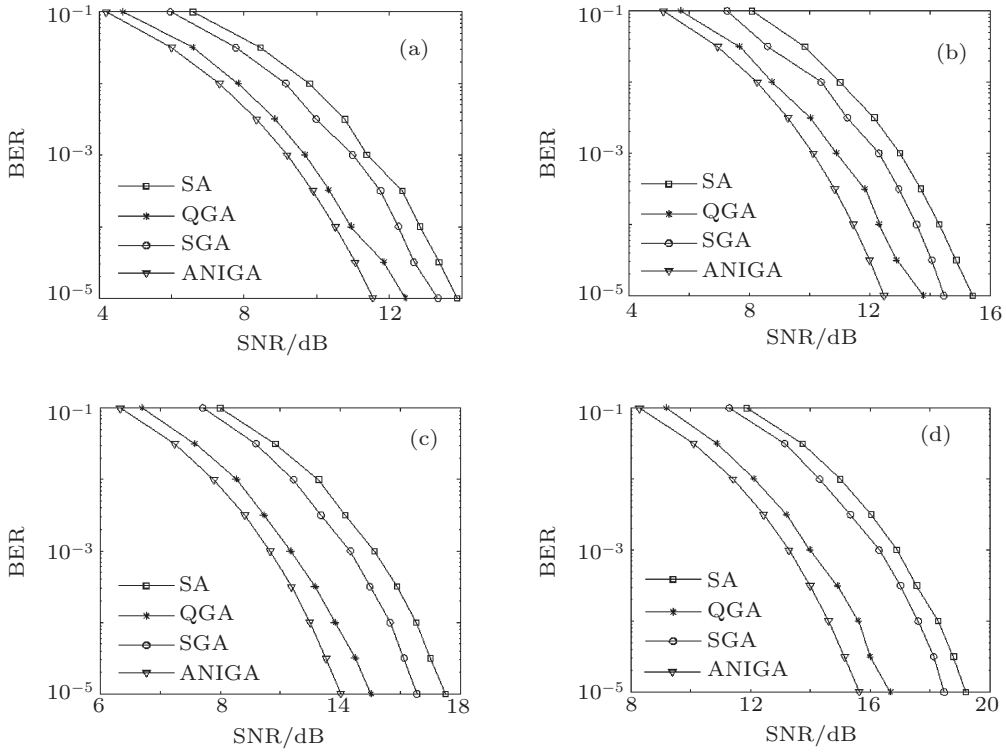


Fig. 5. The bit error rate against the signal-to-noise ratio with the numbers of secondary users: (a) 2, (b) 4, (c) 6 and (d) 8.

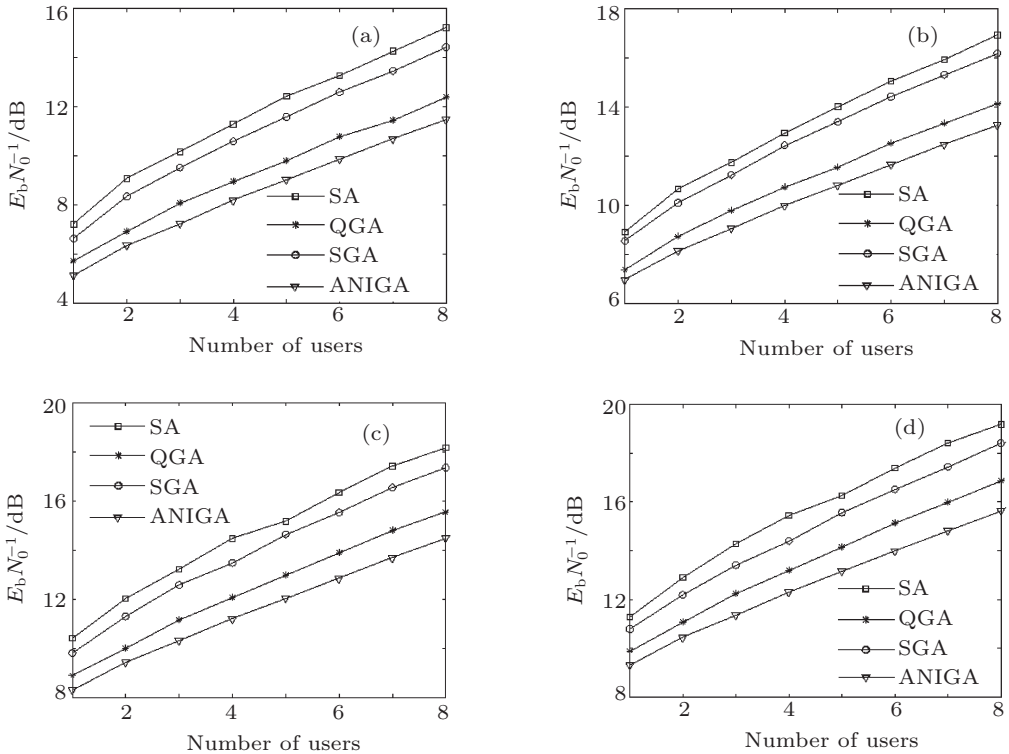


Fig. 6. Variations of E_b/N_0 with the number of secondary users at (a) $P_e = 10^{-2}$, (b) $P_e = 10^{-3}$, (c) $P_e = 10^{-4}$ and (d) $P_e = 10^{-5}$.

Figure 5 shows the variations of the BER with the signal-to-noise ratio (SNR) for different numbers of secondary users. The QGA, SA and SGA are compared with ANIGA with the numbers of secondary users being 2, 4, 6 and 8, respectively. From Fig. 5, we can see that by niche selection and adaptive adjusting the parameters, ANIGA requires less SNR at the same BER limit, which means that it requires less power consumption. The QGA has a lower bit error rate than the SA and SGA at the same SNR. Meanwhile, compared with the other three algorithms, ANIGA reduces the system BER significantly at the same SNR.

Figure 6 shows the variations of $E_{\rm b}/N_0$ with the number of secondary users when BERs are 10^{-2}, 10^{-3}, 10^{-4} and 10^{-5}, respectively. As shown in Fig. 6, the QGA needs lower per-bit energy than the SA and the SGA under the same $E_{\rm b}/N_0$. Compared with the QGA, the SA and the SGA, ANIGA consumes less per-bit energy, which means that the system needs less transmission power. With the increase in the number of secondary users, ANIGA reduces the required $E_{\rm b}/N_0$ from 1 to 3 dB compared with the other three algorithms, which means that ANIGA has more obvious advantages in multi-user cognitive radio networks.

5. Conclusion

In this paper, we presented an adaptive niche immune genetic algorithm for cognitive radio network resource allocation. We also designed the corresponding fitness function and random sequence generator. The simulation results showed that the adaptive niche immune genetic algorithm performs better than the simulated annealing algorithm, the quantum genetic algorithm and the simple genetic algorithm in both convergence speed and global searching capability. The new algorithm improves system power consumption and the bit error rate in multi-user cognitive radio networks.

References

[1] Joseph M III, Gerald Q and Maguire J R 1999 *IEEE Pers. Comm. Mag.* **6** 3

[2] Chantaraskul S and Moessner K 2010 *IET Comm.* **4** 495

[3] Qu Q, Milstein L B and Vaman D R 2008 *IEEE J. Sel. Area. Comm.* **26** 70

[4] Jia J S, Zhang Q and Shen X M, 2008 *IEEE J. Sel. Area. Comm.* **26** 106

[5] Hasan Z, Bansal G, Hossain E and Bhargava V 2009 *IEEE T. Wirel. Comm.* **8** 6078

[6] Ngo D T, Tellambura C and Nguyen H H 2009 *IEEE T. Veh. Technol.* **58** 4878

[7] Sanchez L, Lanza J and Munoz L 2009 *Electron. Lett.* **45** 558

[8] Zhao Z J, Peng Z, Zheng S L, Xu S Y, Lou C Y and Yang X N 2009 *Acta Phys. Sin.* **58** 1358 (in Chinese)

[9] Lou X Y and Cui B T 2008 *Chin. Phys.* B **17** 520

[10] Ma Q L, Zheng Q L, Peng H, Zhong T W and Qin J W 2008 *Chin. Phys.* B **17** 536

[11] Guo W Z and Zhang S 2010 *J. Electro. Infor. Techn.* **32** 1168 (in Chinese)

[12] Ren H P, Han C Z and Liu D 2008 *Chin. Phys.* B **17** 1202

[13] Yang Q T and Gao T G 2008 *Chin. Phys.* B **17** 2388

[14] Zhao Z J, Xu S Y, Zheng S L and Yang X N 2009 *Acta Phys. Sin.* **58** 5118 (in Chinese)

[15] Zhou P and Cao Y X 2007 *Chin. Phys.* **16** 2903

[16] Meng Q F, Peng Y H and Sun J 2007 *Chin. Phys.* **16** 3220

[17] Zhang Q L and Wang S T 2009 *Acta Phys. Sin.* **58** 107 (in Chinese)

[18] Wei D Q and Luo X S 2007 *Chin. Phys.* **16** 3244

[19] Zhang X H and Li D 2009 *Chin. Phys.* B **18** 1774

[20] Zhang R X, Tian G, Li P and Yang S P 2008 *Acta Phys. Sin.* **57** 2073 (in Chinese)

[21] Gu Q L and Gao T G 2009 *Chin. Phys.* B **18** 84

[22] Wu X D and Song Z H 2008 *Chin. Phys.* B **17** 3241

[23] Liu Y Z, Jiang C S and Lin C S 2007 *Acta Phys. Sin.* **56** 707 (in Chinese)

[24] Wang D F and Han P 2008 *Chin. Phys.* B **17** 3603

[25] Wang G Y, Bao X L and Wang Z L 2008 *Chin. Phys.* B **17** 3596

[26] Liu Y F, Yang X G, Miao D and Yuan R P 2007 *Acta Phys. Sin.* **56** 6250 (in Chinese)

[27] Cai G L, Zheng S and Tian L X 2008 *Chin. Phys.* B **17** 2412

[28] Wu W J, Chen Z Q and Yuan Z Z 2008 *Chin. Phys.* B **17** 2420

[29] Wang X Y and Meng J 2009 *Acta Phys. Sin.* **58** 3780 (in Chinese)

[30] Ma S H, Fang J P and Zheng C L 2008 *Chin. Phys.* B **17** 2767

[31] Wang S, Cai L, Kang Q, Wu G and Li Q 2008 *Chin. Phys.* B **17** 2837

[32] Zhu S P, Qian F C and Liu D 2010 *Acta Phys. Sin.* **59** 2250 (in Chinese)

[33] Hui M, Zhang Y B and Liu C X 2008 *Chin. Phys.* B **17** 3258

[34] Zhang J Z, Wang Y C and Wang A B 2008 *Chin. Phys.* B **17** 3264

[35] Zong X P, Xu Y and Dong J T 2006 *Acta Phys. Sin.* **55** 3223 (in Chinese)

[36] Long M, Peng F and Chen G R 2008 *Chin. Phys.* B **17** 3588

[37] Zhang H G, Ma T D, Yu W and Fu J 2008 *Chin. Phys.* B **17** 3616

[38] Meng J and Wang X Y 2009 *Acta Phys. Sin.* **58** 819 (in Chinese)

[39] Wang G Y and He H L 2008 *Chin. Phys.* B **17** 4014

[40] Bao B C, Li C B, Xu J P and Liu Z 2008 *Chin. Phys.* B **17** 4022

[41] Wang Y, Zhai H C and Mu G G 2005 *Acta Phys. Sin.* **54** 1965 (in Chinese)

[42] Xu S J, Wang J Z and Yang S X 2008 *Chin. Phys.* B **17** 4027
[43] Cai G L, Zheng S and Tian L X 2008 *Chin. Phys.* B **17** 4039
[44] Zhang R X and Yang S P 2008 *Chin. Phys.* B **17** 4073
[45] Zhou H, Li H Y, Gao S, Zhang Y H, Jia Z M and Lin S L 2008 *Chin. Phys.* B **17** 4428
[46] Tu S Y, Chen K C and Prasad R 2009 *IEEE T. Veh. Technol.* **58** 3410
[47] Zhao Z J, Zheng S L, Shang J N and Kong X Z 2007 *Acta Phys. Sin.* **56** 6760 (in Chinese)
[48] Zhao Z J, Peng Z, Zheng S L and Shang J N 2009 *IEEE T. Wirel. Comm.* **8** 4421
[49] Zheng S L, Lou C Y and Yang X N 2010 *Acta Phys. Sin.* **59** 3611 (in Chinese)
[50] Song D and Zhang X L 2010 *Acta Phys. Sin.* **59** 6697 (in Chinese)
[51] Zu Y X, Zhou J and Zeng C C 2010 *Chin. Phys.* B **19** 119501
[52] Zhou J and Zu Y X 2010 *Acta Phys. Sin.* **59** 7508 (in Chinese)
[53] Li Y L, Wang M J and Dong Q F 2010 *Chin. Phys.* B **19** 115204
[54] Tang Z J and He Y G 2009 *Acta Phys. Sin.* **58** 5126 (in Chinese)
[55] Li Y L and Wang M J 2009 *Chin. Phys.* B **18** 2420
[56] Liu Q J, Yang L, Wang J Y, Zuo H Y, Luo S R and Andrew Y S C 2009 *Acta Phys. Sin.* **58** 7376 (in Chinese)